# Supporting Information for "Very-long-period seismicity over the 2008-2018 eruption of Kīlauea Volcano"

**Josh Crozier**[1], **Leif Karlstrom**[1]

[1]Department of Earth Sciences, University of Oregon, Eugene, Oregon, USA.

## Contents

Figures S.1 to S.24, arranged in sections 1: Synthetic waveform test figures, 2: Catalog figures, and 3: Example event figures

## Additional Supporting Information (Files uploaded separately)

1. *Kilauea_2008-2018_resonant_signal_catalog_presented.csv*

   A version of our event catalog thresholded to include 3209 events, as presented in the text. The first row contains descriptions of each variable, and the second row contains the names of each variable.

2. *Kilauea_2008-2018_resonant_signal_catalog_full.csv*

   A version of our event catalog thresholded to include 33084 events. The thresholds used in this version are: STA/LTA > 2, standard deviations above the LTA > 1, $Q$ > 4, and mean phase deviation < 0.25 radians. The first row contains descriptions of each variable, and the second row contains the names of each variable.

## 1 Synthetic waveform test figures

Corresponding author: Josh Crozier, jcrozier@uoregon.edu

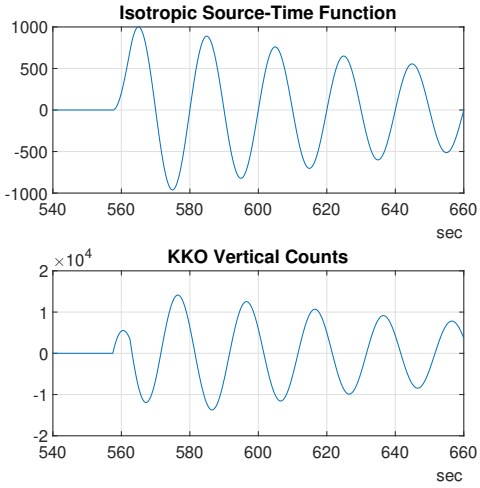


**Figure S.1.** Example synthetic source-time function and corresponding synthetic seismogram (which has been convolved with the elastic Green's functions and instrument response), zoomed in around the signal onset to show the tapers used (see appendix). This source-time function is for an impulsive onset oscillation with $T$ = 20 s, $Q$ = 20, and no added noise.

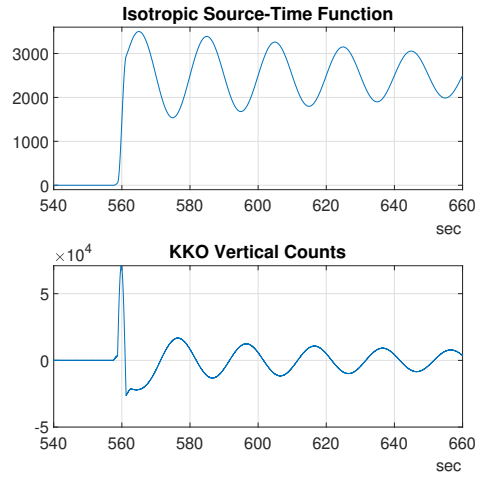


**Figure S.2.** Example synthetic source-time function and corresponding synthetic seismogram (which has been convolved with the elastic Green's functions and instrument response), zoomed in around the signal onset to show the tapers used (see appendix). This source-time function is for an impulsive onset oscillation with $T$ = 20 s, $Q$ = 20, an added step displacement, and no added noise.

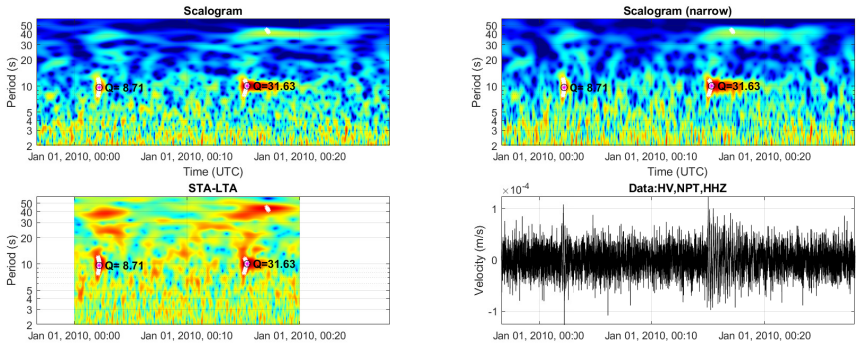


**Figure S.3.** Example scalograms and detected resonant signals from a synthetic seismogram consisting of four resonant signals with [start time, $T$, $Q$] = [00:05, 40, 6], [00:05, 10, 6], [00:15, 40, 40], [00:15, 40, 40], plus white noise from a standard normal distribution scaled by 5.0% of the signal amplitude. At this noise level only two of the signals are found at the detection thresholds used, and the quality factor estimates are less accurate (off by ~25%).

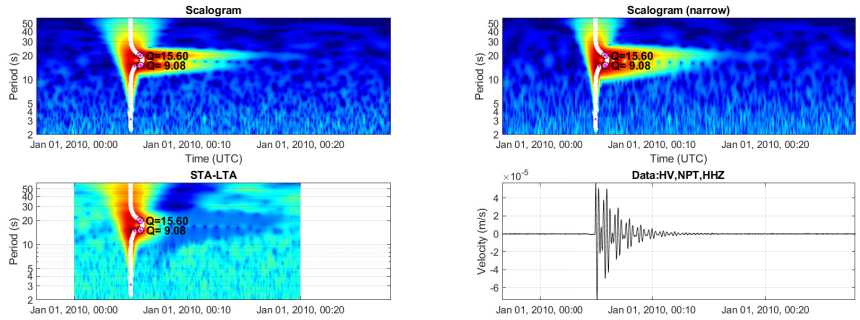


**Figure S.4.** Example scalograms and detected resonant signals from a synthetic seismogram consisting of two resonant signals with [start time, $T$, $Q$] = [00:05, 20, 20], [00:05, 15, 20], plus white noise from a standard normal distribution scaled by 0.1% of the signal amplitude. In this case the spectral proximity of the two signals means that wavelets at the period of one signal are influenced by the other signal, which causes both quality factors to be under-estimated (by 22-54%).

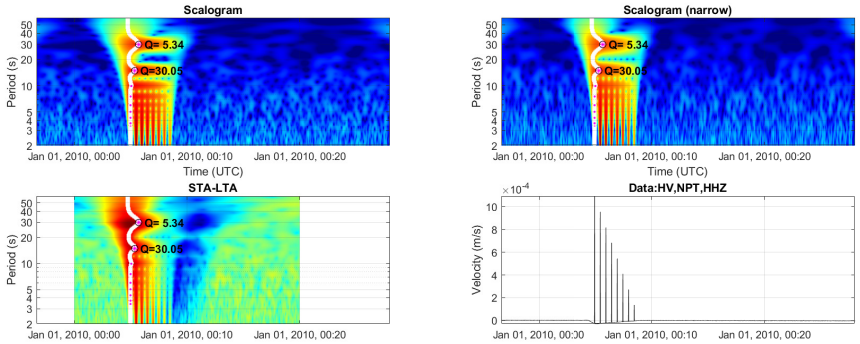


**Figure S.5.** Example scalograms and detected resonant signals from a synthetic seismogram consisting of eight step displacements (velocity spikes) spaced 30 s apart, plus white noise from a standard normal distribution scaled by 1.0% of the signal amplitude. The closely spaced spikes create a Dirac comb effect, where the spectrum would indicate apparent resonances at 15 s, 7.5 s, 3.25 s, and etc. The temporal resolution of our narrow ($\beta$=20) wavelet, which is used for calculating $Q$, is high enough that apparent resonances with $T$ less than 15 s are not picked.

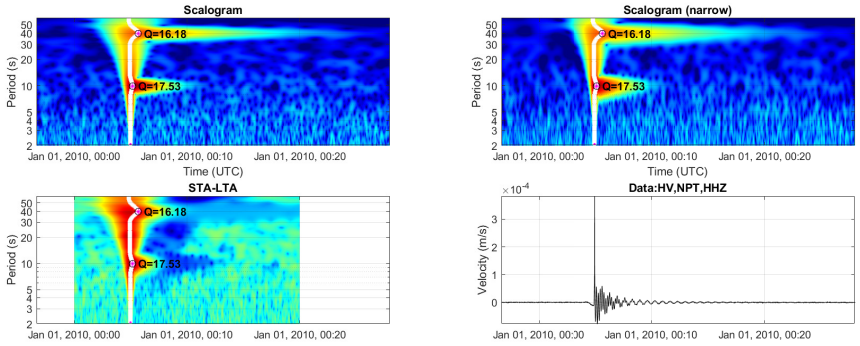


**Figure S.6.** Example scalograms and detected resonant signals from a synthetic seismogram consisting of a large step displacement (velocity spike) at time 00:05 plus two resonant signals with [start time, $T$, $Q$] = [00:05, 40, 20] and [00:05, 10, 20] plus white noise from a standard normal distribution scaled by 0.1% of the signal amplitude. The presence of the step function decreases the estimated quality factors by 12-19% due to the increased energy at the start of the signals, but otherwise does not appreciably impact the results.

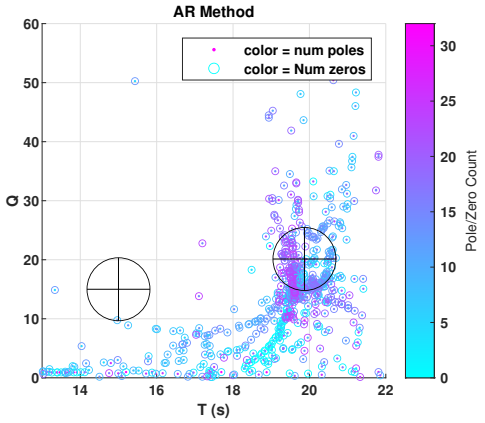


**Figure S.7.** Example 'Sompi' AR method for estimating $T$ and $Q$ applied to a synthetic seismogram. Code used from Lesage 2009. In this case the method was applied to a data window from 10-200 s following the onset of a 20 s oscillation with $Q$ = 20 and a smaller (by a factor of 4) 15 s oscillation with $Q$ = 15 (indicated by black crosses/circles). Results from filters with 4-32 poles and 0-32 zeros are shown to test a wide parameter space; for practical use narrower ranges would likely be used. A cluster near the actual $T$ and $Q$ of the 20 s oscillation does occur, though mean $T$ and $Q$ values within this cluster are offset from the correct value and exhibit significant scatter. No cluster occurs near the smaller 15 s oscillation, so it would be missed entirely by this AR method.

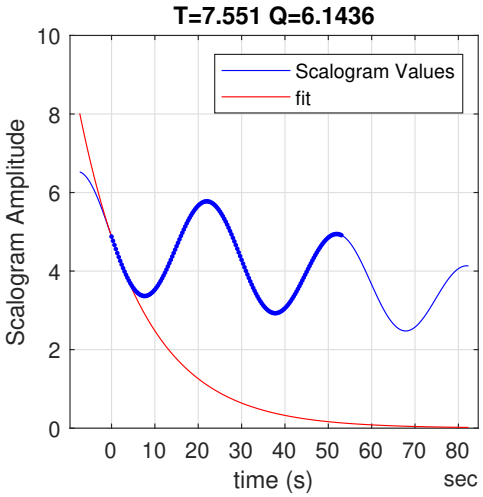


**Figure S.8.** Example estimation of $Q$ by scalogram exponential fit. Applied to synthetic seismograms consisting of a series of tapered step displacements (velocity spikes) spaced 30 s apart, plus white noise from a standard normal distribution scaled by 0.1% of the signal amplitude. The closely spaced spikes create a Dirac comb effect, where the frequency spectrum would indicate apparent resonances at 15 s, 7.5 s, 3.25 s, and etc. The time resolution of the $\beta$=20 wavelet we use for calculating $Q$ is sufficient to distinguish gaps in this apparent 7.5 s resonance, so our fit avoids overestimating $Q$ as a standard least-squares exponential regression would.

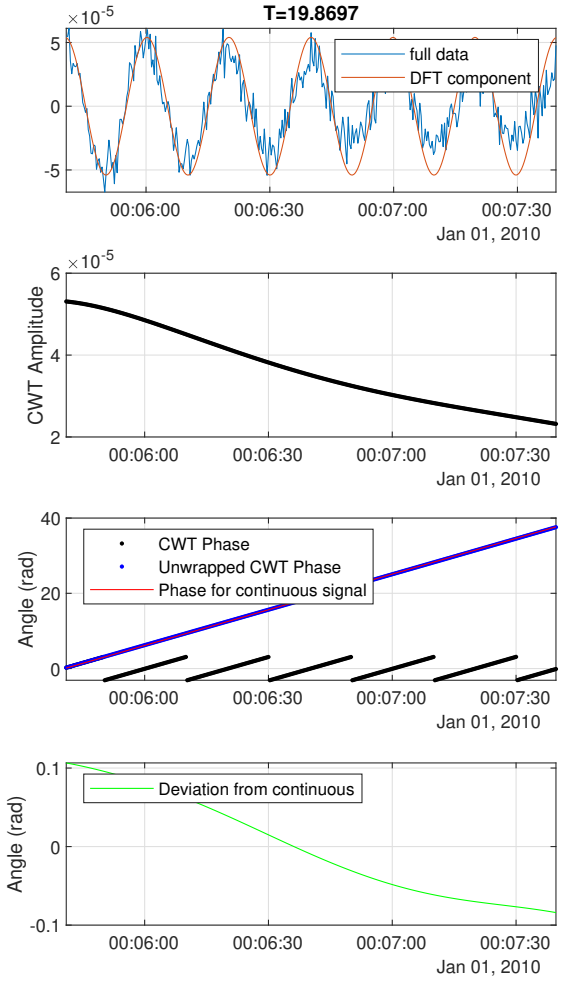


**Figure S.9.** Example phase continuity from a synthetic seismogram consisting of a resonant signal with $T$=20 s and $Q$=20, plus white noise from a standard normal distribution scaled by 0.1% of the signal amplitude. In this case the phase deviation is small (mean of around 0.05 radians), correctly indicating that this is likely a continuous oscillation.

## 2 Catalog figures

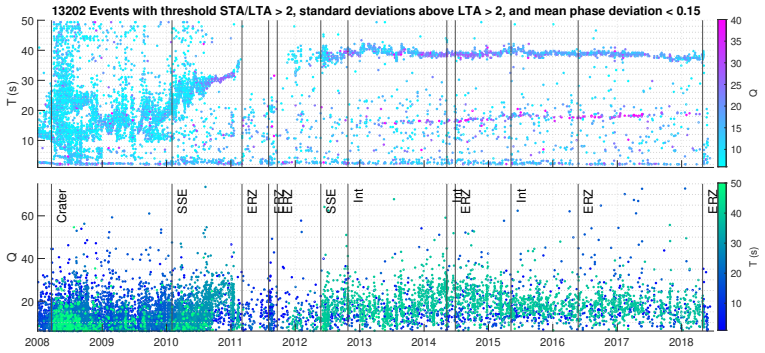


**Figure S.10.** Resonant signal catalog from 2008-2018 with less strict event detection thresholds than presented in the main text. 'Crater' indicates where the Halema'uma'u crater first formed, 'SSE' indicates slow slip events, 'Int' indicates documented summit intrusions, and 'ERZ' indicates eruptions along the East-Rift-Zone.

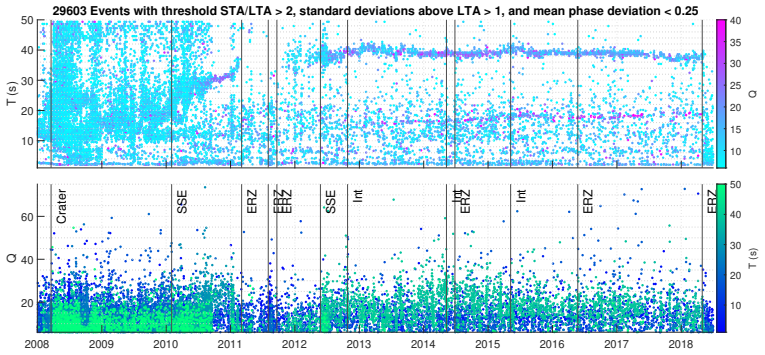


**Figure S.11.** Resonant signal catalog from 2008-2018 with less strict event detection thresholds than presented in the main text. 'Crater' indicates where the Halema'uma'u crater first formed, 'SSE' indicates slow slip events, 'Int' indicates documented summit intrusions, and 'ERZ' indicates eruptions along the East-Rift-Zone.

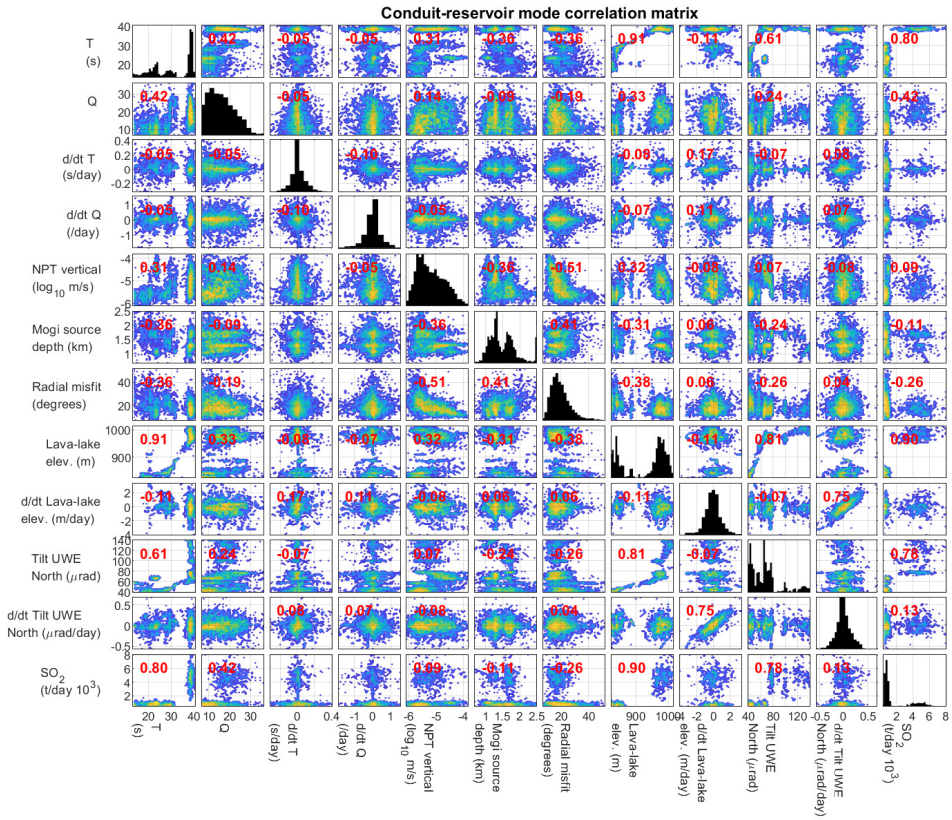


**Figure S.12.** Conduit-reservoir mode correlation matrices from 2008-2018. Off-diagonal plots are colored by the logarithm of the number of points in a given parameter bin, and histograms on diagonal plots show the distribution of each parameter. Red numbers are Pearson's correlation coefficients, only shown for correlations with P-values less than 0.05. All time derivatives were calculated with a 7-day cutoff-period differentiator filter (see Methods section).

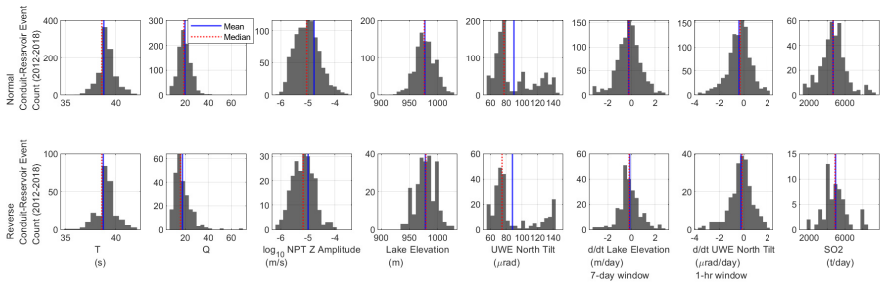


**Figure S.13.** Histograms of Normal and Reverse conduit-reservoir mode event parameters from 2012-2018.

## 3 Example event figures

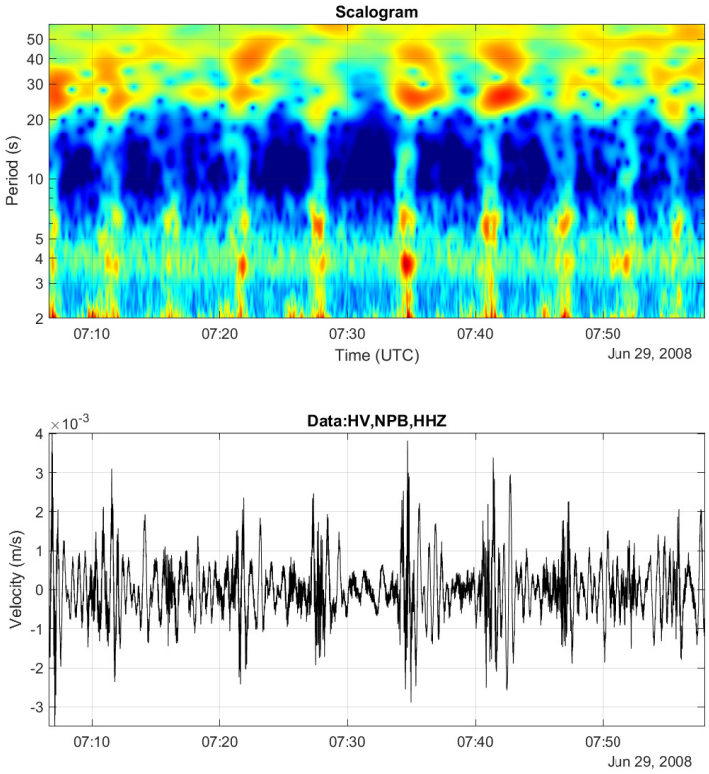


**Figure S.14.** VLP events with regular recurrence interval from June 2008, a few months after the Overlook Crater began forming. These events occurred roughly every 5 minutes and contained broadband energy with spectral peaks at around 3.5 s, 6 s, 25 s, and possibly 40 s. These events exhibited less clear onsets and exponential decays than typical rockfall-triggered events.

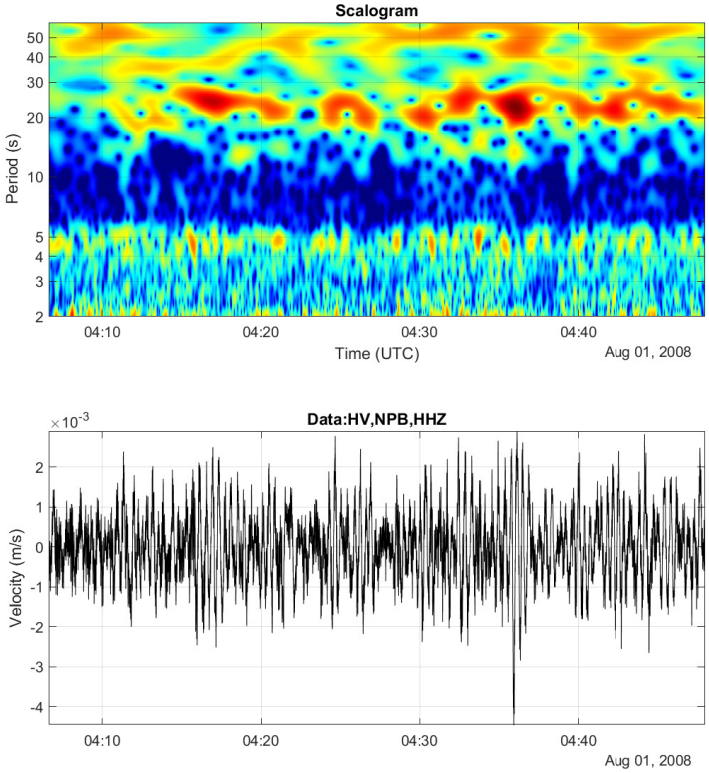


**Figure S.15.** VLP tremor from August 2008, in the first focused cluster of VLP signals. There was elevated energy at periods from 15-30 s and 4-5 s, though the dominant periods were not clearly focused and were variable over time. The signal cannot readily be separated into distinct events, and exhibited no clear high frequency triggers.

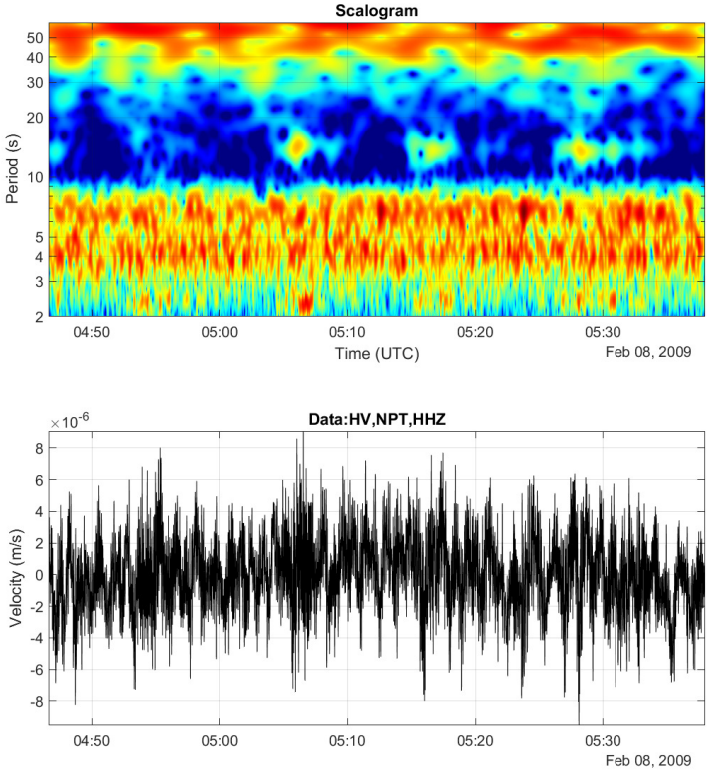


**Figure S.16.** VLP events from February 2009, around the time where dominant VLP period is at a minimum. These appear to be distinct VLP events, thought onsets of some were gradual and first motions were not well defined. Elevated energy at periods < 2 s occurred alongside these signals, but did not appear to represent the more broadband impulsive trigger mechanisms that occur at the onset of typical rockfall events.

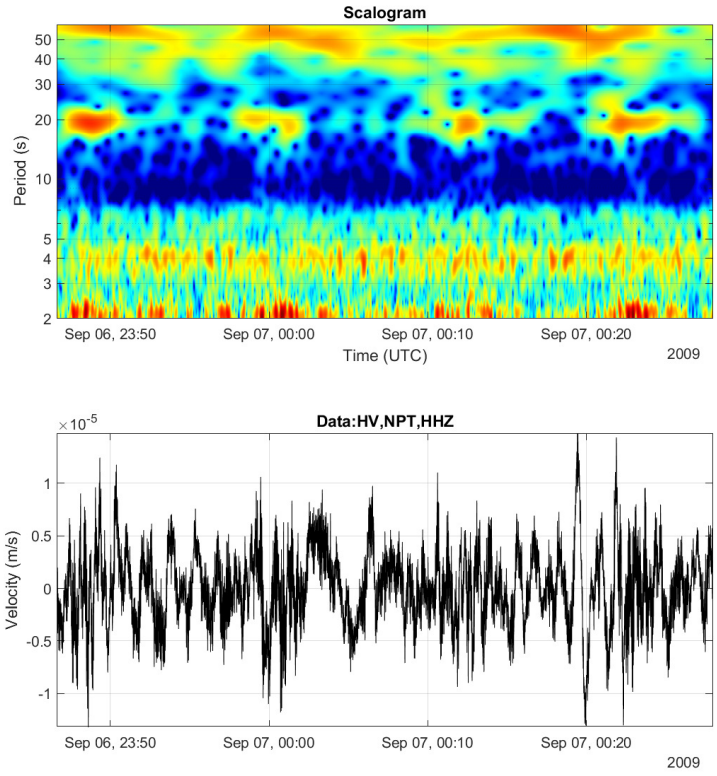


**Figure S.17.** VLP tremor from September 2009, in a signal cluster that seems to represent a local maxima in VLP period (around 20 s).

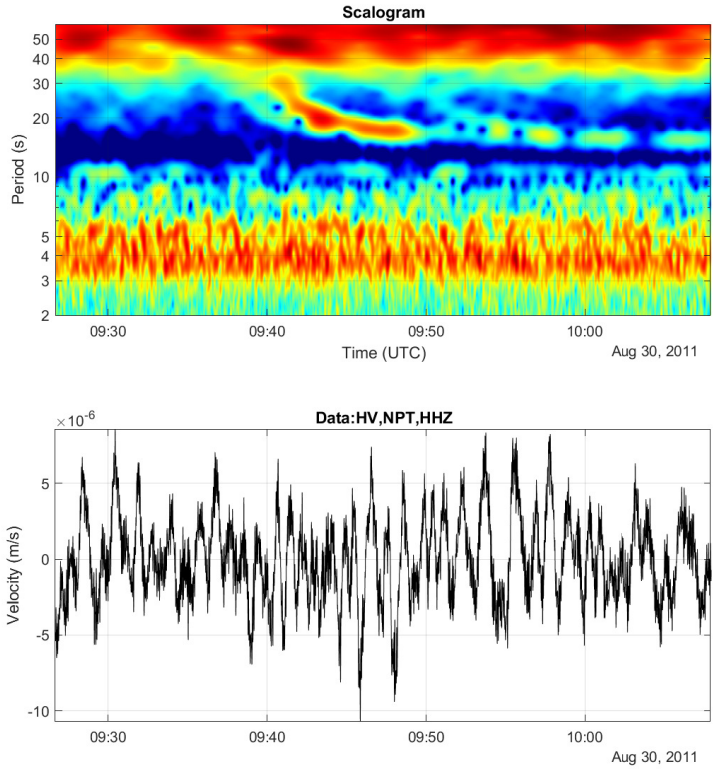


**Figure S.18.** Gliding-frequency VLP signal from August 2011, part of a small cluster of VLP seismicity following the August 2011 Pu‘u ‘Ō‘ō eruption. This event had no apparent high frequency trigger. VLP energy remained elevated for 10s of minutes after the event, though this energy did not appear to represent continuous decay of the initial resonance but rather continued intermittent forcing, perhaps partly by what may be a second smaller gliding-frequency signal around 10 minutes after the first. There was also background VLP tremor present with a period of around 11 s that does not appear to have been effected by the gliding-frequency event.

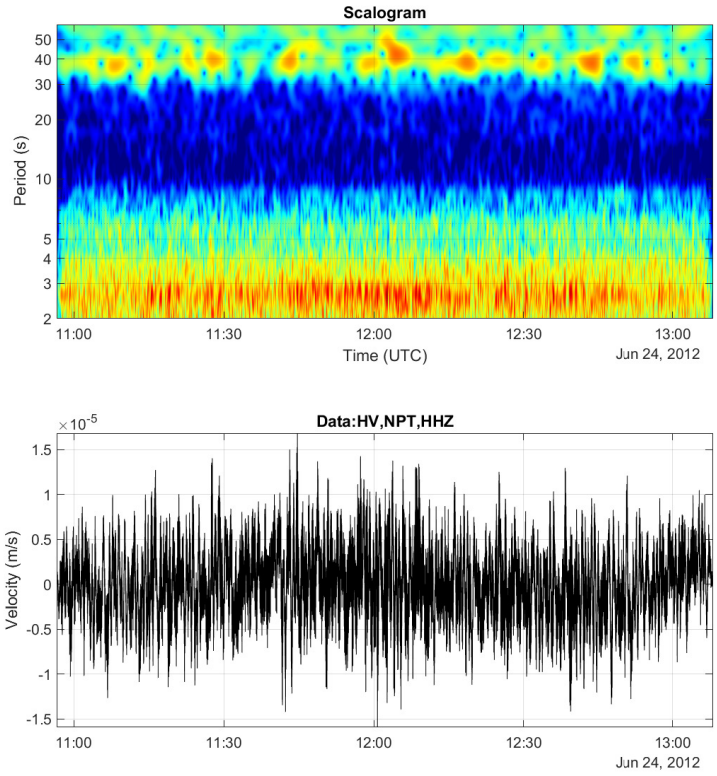


**Figure S.19.** VLP tremor from June 2012, shortly after the May SSE and around when higher $Q$ VLP events start occurring again after a year with minimal VLP seismicity.

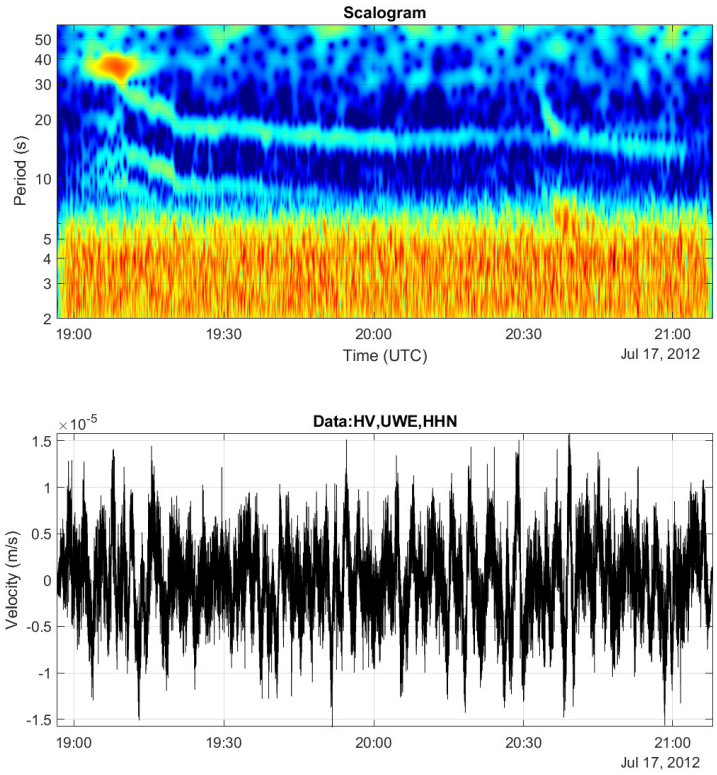


**Figure S.20.** Gliding-frequency VLP signals from July 2012. There was a set of three resonant modes starting around 19:10, and a single resonant mode that started about 90 minutes later. No high frequency triggers were apparent. The first 3 modes all exhibited a similar glide to lower periods over about 10 minutes, then maintained more stable periods. The later mode had a more rapid initial glide to lower periods (over about 5 minutes) but then continued more slowly gliding for another 20 minutes.

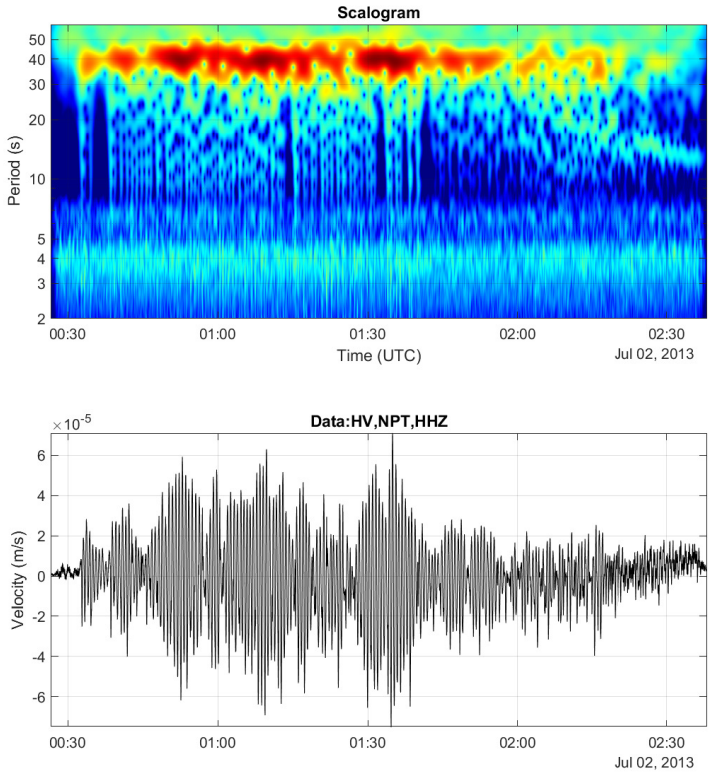


**Figure S.21.** VLP event/tremor from July 2013. This signal consisted of sustained 40 s oscillations at varying amplitudes and irregular bursts of higher frequency energy. These bursts were much weaker relative to the main VLP oscillation than typical rockfall trigger signals. The main VLP signal had an impulsive onset with deflationary first motions.

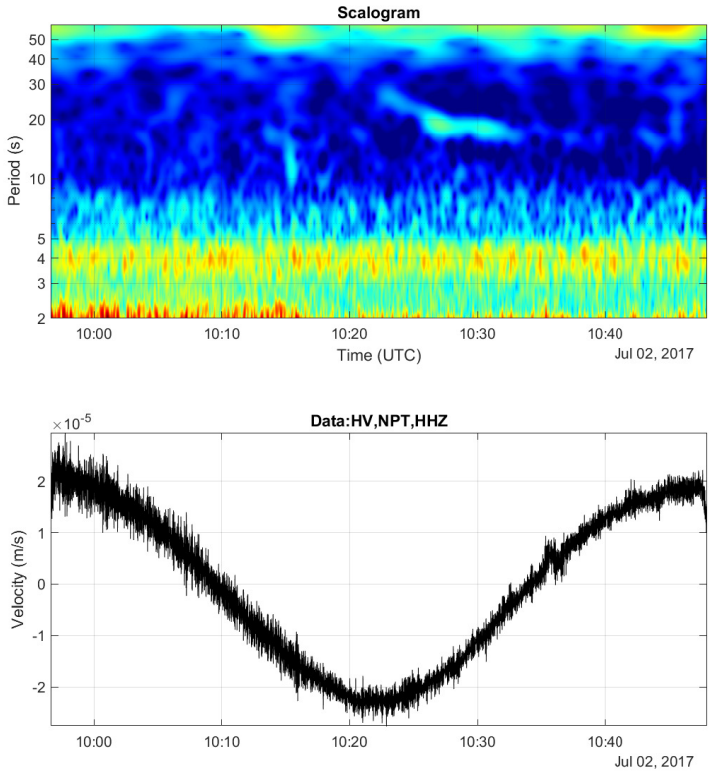


**Figure S.22.** Isolated lake sloshing mode with possible gliding-frequency onset from July 2017.

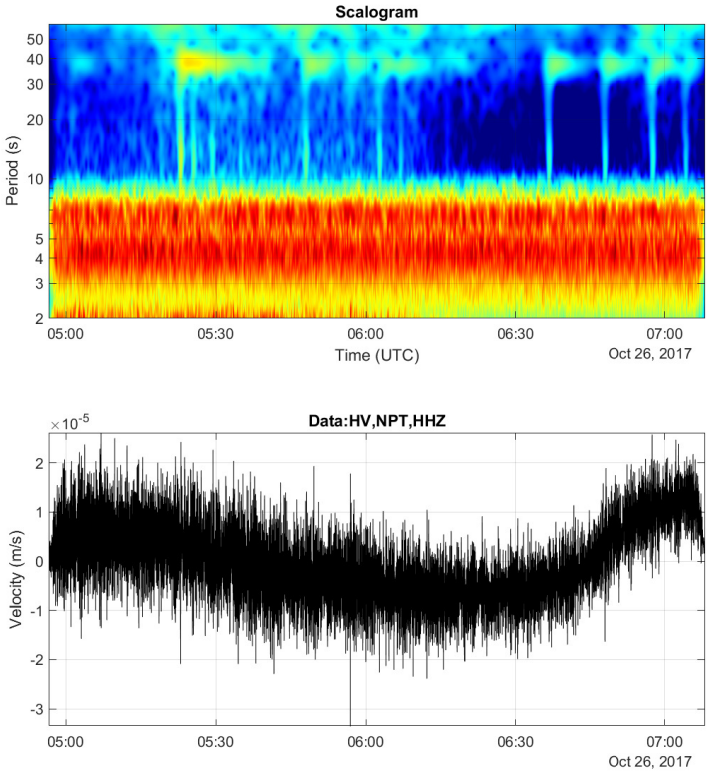


**Figure S.23.** Closely spaced Normal conduit-reservoir events from October 2017. These may have represented a series of small rockfalls.

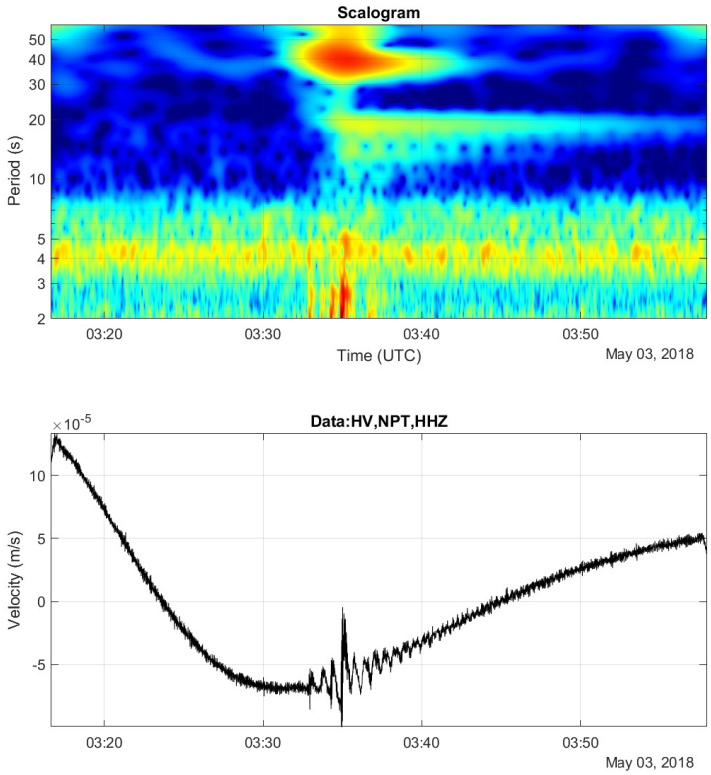


**Figure S.24.** VLP event with two clear lava-lake-sloshing modes from May 2018, a day after the lava-lake began draining. The dominant 40 s mode for this event started with impulsive inflationary motions, though with only a very faint high frequency trigger, but then grew for several minutes until a second impulse occurred and exponential decay began. The lava-lake-sloshing modes appeared alongside this second impulse.